Unified Near-Field and Far-Field Localization for AOA and Hybrid AOA-TDOA Positionings

Yue Wang, *Student Member, IEEE*, and K. C. Ho, *Fellow, IEEE*

***Abstract*— Point positioning of a signal source is feasible if it is not far from the sensors and direction of arrival (DOA) localization is only applicable if it is distant. Point positioning and DOA localization employ different estimation models and prior knowledge about the source range is often not available to decide which model is appropriate. This paper introduces the modified polar representation to unify the localization of a source using angle of arrival (AOA) regardless if it is near or far. From the Gaussian AOA measurements, we utilize the hybrid Bhattacharyya-Barankin (HBB) bound to illustrate it is not possible to obtain the Cartesian coordinates of a distant source when applying the near-field model, and derive the DOA bias of a not so distant source when using the far-field model. An iterative maximum likelihood estimator (MLE) is next derived under the modified polar representation with a single model, where the HBB bound confirms the stable behavior of the estimator regardless it is near or far. The algorithm yields a position if the source is close and a DOA if it is distant. A preliminary solution to initialize the MLE using semidefinite relaxation is also proposed. The HBB bound, the analysis and the algorithm are extended for hybrid AOA-TDOA localization.**

***Index Terms*— AOA, AOA-TDOA, DOA estimation, HBB bound, localization, source positioning.**

I. Introduction

THE applications of wireless sensor network (WSN) are immense, extending from environmental monitoring, smart building, predictive maintenance, to traffic monitoring and asset tracking [1]–[10]. A fundamental task for the various applications is to determine the location of an object (simply called source) using the signal it reflects or radiates. This is accomplished by acquiring the source signal at the sensors, obtaining the positioning parameters and solving a non-linear optimization problem.

A popular positioning parameter for WSN is the angle of arrival (AOA) [11]–[19]. AOA indicates the direction of the source signal arriving at a sensor and it defines a straight line passing through the source. Obtaining AOA often involves a little sophisticated sensor that is equipped with an array of receivers. On the other hand, it does not require synchronization among the sensors [9], [20], [21] and data communication between them is minimal as each sensor produces the angle itself. A time (range) based positioning parameter is the time-difference of arrival (TDOA) [22]–[24]. It is the arrival time difference of the source signal in reaching two sensors and it forms a hyperbolic surface the source lies. TDOA requires synchronization among sensors. It also demands considerable transmission between nodes as cross-correlation of the signals from two sensors is needed.

A central unit integrates the information of the positioning parameters and sensor positions together to yield the source location. It essentially solves a set of non-linear equations for the intersection. The location can be uniquely evaluated to a single coordinate point when the source is near the sensors where the wavefront is curved. On the other hand, the source location can only be characterized by the Direction of Arrival (DOA) when it is distant from the sensors where the wavefront has negligible curvature and becomes linear. For ease of exposition, we consider here the source is in the far field if the source range to the array aperture ratio is large, otherwise it is in the near field. The source range is the distance from the source to the centroid of the array and the array aperture is the maximum separation between two array receivers.

Point positioning and DOA localization process the observations differently, that remains to be the case even in the one-step approach [25]–[28] in obtaining the source location directly from the sensor signal measurements. *A priori* knowledge is needed if the source is in the near field or the far field in order to apply proper algorithm for localization. Such knowledge, unfortunately, is often not available in practice. The Geometric Dilution of Precision (GDOP) [29] may help to decide when to use near or far field technique for localization, if the region where the source is expected to appear is known. It may be reasonable to apply point positioning first and then DOA localization if it fails. Nevertheless, when the source is sufficiently far that point positioning fails and not nearly as distant to satisfy the linear wavefront approximation, the obtained DOA will have a significant amount of bias.

This paper proposes a unified solution with a single model to locate the source using AOA, without requiring the knowledge if the source is near to the sensors or far away. The estimator will yield the point coordinates if it is near and the DOA if it is distant. It will not have the large bias from the far field DOA estimation when the signal wavefront does not appear linear.

The main focus is for AOA observations. We also extend the work for the hybrid AOA and TDOA positioning [24], [30]

Manuscript received May 13, 2017; revised September 16, 2017; accepted November 10, 2017. Date of publication December 4, 2017; date of current version February 9, 2018. The associate editor coordinating the review of this paper and approving it for publication was A. J. Weiss. *(Corresponding author: K. C. Ho.)*

The authors are with the Electrical Engineering and Computer Science Department, University of Missouri, Columbia, MO 65211 USA (e-mail: yw67d@mail.missouri.edu; hod@missouri.edu)

Digital Object Identifier 10.1109/TWC.2017.2777457

where the sensors are synchronized and transmission resources are available. The hybrid system can yield better localization accuracy than using AOA alone or reduce the number of sensors used. Nevertheless, we would like to emphasize that acquiring AOA is more efficient for a narrowband signal otherwise a more computationally demanding approach is needed to obtain AOA in the broadband case. On the other hand, TDOA demands a wideband signal to achieve good accuracy. The signal bandwidth could be a factor for consideration in deciding to use one or both measurements for positioning.

We begin by using the Cramer-Rao Lower Bound (CRLB) and the Hybrid Bhattacharyya-Barankin (HBB) Bound to illustrate that point positioning is not possible as the source range becomes large. Analysis follows to show a significant amount of bias is resulted from far field DOA estimation when the source is not sufficiently distant. We then proceed to develop the proposed algorithm. It is based on the modified polar representation (MPR) of the source position, which is the polar representation except using the inverse-range instead of range. The associated Maximum Likelihood Estimator (MLE) through the Gauss-Newton iteration is derived. The iteration starts with the proposed initial solution that is developed based on the semidefinite relaxation (SDR) technique. Furthermore, the analysis and algorithm developments for AOA are extended to the hybrid AOA and TDOA case.

The study in this paper is new. The related work [31] looks at TDOA measurements only. [32] presented an array processing algorithm for locating a mix of near and far field narrowband sources. It used a completely different approach and is for the DOA estimation only. We have not come across other works in the literature to address the localization problem of a point source without requiring the *a priori* knowledge if it is near or far.

The contributions of this paper include the following for AOA positioning and for hybrid AOA-TDOA localization:

- the HBB Bound evaluation and analysis for point positioning;
- the DOA bias analysis of a distant source from the far-field model;
- the MPR model for localization;
- an iterative MLE for the source location under MPR regardless of the source range;
- an MPR position estimate based on SDR and convex optimization for initializing the MLE.

For the rest of the paper, we shall use the common convention that bold upper and lower case letters represent matrix and column vector. $\mathbf{1}$ and $\mathbf{0}$ are vectors of 1 and 0, and $\mathbf{I}$ and $\mathbf{O}$ are identity and zero matrices. $\mathrm{tr}(\bullet)$ is the trace operation of a matrix. $\|\mathbf{a}\|$ is the Euclidean norm and $\mathbf{a}(i:j)$ is a subvector containing the i-th to the j-th element of $\mathbf{a}$. $\mathbf{A}(i,:)$ and $\mathbf{A}(:,j)$ denote the i-th row and the j-th column of $\mathbf{A}$. $(\bullet)^o$ is the value of the variable $(\bullet)$ evaluated at the true source location and $\Delta(\bullet) = (\bullet) - (\bullet)^o$ is the difference. $\mathbf{A} \succeq 0$ indicates $\mathbf{A}$ is positive semidefinite (PSD). S^N is the set of all real symmetric $N \times N$ matrices. $\tan^{-1}(\bullet)$ is the arc-tangent operation that takes the quadrant into account.

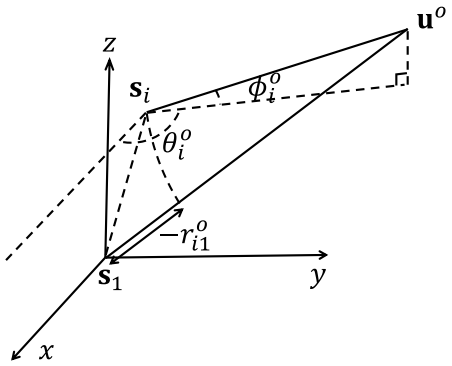

Fig. 1. Near-field localization model.

II. Localization Scenario

Let us assume a three-dimensional (3-D) WSN that has M sensors distributed randomly at $\mathbf{s}_i = [x_i, y_i, z_i]^T$, $i = 1, \ldots, M$. Without loss of generality the first sensor is set as the origin so that $\mathbf{s}_1 = [0, 0, 0]^T$. The WSN is intended to estimate the location of a signal source whose true position is denoted by $\mathbf{u}^o = [x^o, y^o, z^o]^T$. Each sensor acquires the AOA of the source signal that is represented by the azimuth and elevation angle pair (θ_i, ϕ_i) as shown in Fig. 1. The true angle values in terms of the source position are

$$\theta_i^o = \tan^{-1}\left(\frac{y^o - y_i}{x^o - x_i}\right)$$
$$\phi_i^o = \tan^{-1}\left(\frac{z^o - z_i}{(x^o - x_i)\cos\theta_i^o + (y^o - y_i)\sin\theta_i^o}\right) \quad (1)$$

Collecting the azimuth and elevation angles from all the sensors, the AOA measurement model is

$$\mathbf{a} = [\boldsymbol{\theta}^T, \boldsymbol{\phi}^T]^T = \mathbf{a}^o + \mathbf{n_a}, \quad \mathcal{N}(\mathbf{0}, \mathbf{Q_a}). \quad (2)$$

In addition to AOA, the sensors are also capable of obtaining TDOAs. We use the first sensor as the reference for TDOA so that after multiplying with the signal propagation speed, the true TDOA between the sensor pair i and 1 is related to the source position by

$$r_{i1}^o = \|\mathbf{u}^o - \mathbf{s}_i\| - \|\mathbf{u}^o - \mathbf{s}_1\|. \quad (3)$$

r_{i1}^o is the range difference to be exact. The range difference and TDOA are used interchangably here since the two are differed by a constant scaling factor. The measurement model for the collection of the TDOAs $\mathbf{r} = [r_{21}, r_{31}, \cdots, r_{M1}]^T$ is

$$\mathbf{r} = \mathbf{r}^o + \mathbf{n_r}, \quad \mathcal{N}(\mathbf{0}, \mathbf{Q_r}). \quad (4)$$

The total set of measurements is

$$\mathbf{m} = [\mathbf{a}^T, \mathbf{r}^T]^T = \mathbf{m}^o + \mathbf{n}, \quad \mathcal{N}(\mathbf{0}, \mathbf{Q_m}). \quad (5)$$

where $\mathbf{Q_m}$ has diagonal blocks $\mathbf{Q_a}$ and $\mathbf{Q_r}$, and the off-diagonal blocks correspond to the correlation between the AOA and TDOA measurements.

The interest is to estimate the source location $\mathbf{u}^o$ using the AOA measurements $\mathbf{a}$ or the hybrid measurements $\mathbf{m}$, where the prior knowledge about the source range is not available to indicate if the source is near or far.

The proposed solutions derived below use a 3-D scenario. The solution for 2-D localization can be deduced from the 3-D solution by ignoring the z-coordinate. The sensors and source positions described above are in the Cartesian coordinates. In polar coordinates, they are denoted by $\mathbf{s}_i = [\alpha_i, \beta_i, R_i]^T$ and $\mathbf{u}^o = [\theta^o, \phi^o, r^o]^T$, where α_i and θ^o correspond to the azimuth angles, β_i and ϕ^o the elevation angles, and R_i and r^o the ranges with respect to $\mathbf{s}_1$ (the origin).

To simplify the exposition, we shall assume the sensor positions are exact without error, which may not be the case in WSN. Nevertheless, it is straightforward to generalize the studies and results presented here directly to include the sensor position errors.

III. AOA Localization Analysis

A. Localization in Near-Field

When the source is not far away from the sensors, we can adopt the near field model depicted in Fig. 1 to locate the source. The near field model assumes the radial lines from the sensors defined by the AOAs intersect, yielding a point position of the source. From (2), the MLE for $\mathbf{u}^o$ is the minimizer of the cost function

$$J_{n,a}(\mathbf{u}) = (\mathbf{a} - \tilde{\mathbf{a}}(\mathbf{u}))^T \mathbf{Q}_\mathbf{a}^{-1} (\mathbf{a} - \tilde{\mathbf{a}}(\mathbf{u})) \tag{6}$$

where $\tilde{\mathbf{a}}(\mathbf{u})$ is the reconstructed angle values according to (1) by replacing the true value $\mathbf{u}^o$ with the optimization variable $\mathbf{u}$. $J_{n,a}$ is a complicated function of $\mathbf{u}$ and it does not have an analytic solution. A common approach for minimizing (6) is through iteration using the Gauss-Newton method.

Linearizing $\tilde{\mathbf{a}}(\mathbf{u})$ by the Taylor-series expansion at some initial value $\mathbf{u}^{(0)}$ and ignoring the higher order terms give a quadratic approximation of $J_{n,a}(\mathbf{u})$. Taking gradient and setting it to zero yield a solution that we can iterate to reduce the linearization error, resulting in the Gauss-Newton iterative equation for solving the unknown,

$$\mathbf{u}^{(k+1)} = \mathbf{u}^{(k)} + (\mathbf{G}_\mathbf{a}^{(k)T}\mathbf{W}\mathbf{G}_\mathbf{a}^{(k)})^{-1}\mathbf{G}_\mathbf{a}^{(k)T}\mathbf{W}(\mathbf{a} - \tilde{\mathbf{a}}^{(k)}), \quad k = 0, 1, \ldots \tag{7}$$

$\mathbf{u}^{(k)}$ represents the source location estimate after k iterations, $\mathbf{W} = \mathbf{Q}_\mathbf{a}^{-1}$ and $\tilde{\mathbf{a}}^{(k)}$ is the AOA vector constructed from $\mathbf{u}^{(k)}$ using (1). The variable

$$\mathbf{G}_\mathbf{a}^{(k)} = [\mathbf{G}_{\boldsymbol{\theta}}^{(k)T}, \mathbf{G}_{\boldsymbol{\phi}}^{(k)T}]^T \tag{8}$$

is the Jacobian matrix of azimuth and elevation angles. From the relationships (1), the i-th row of $\mathbf{G}_{\boldsymbol{\theta}}^{(k)}$ is

$$\mathbf{G}_{\boldsymbol{\theta}}^{(k)}(i,:) = \left[-\frac{y^{(k)} - y_i}{r_i^{(k)2}\cos^2\phi_i^{(k)}} \quad \frac{x^{(k)} - x_i}{r_i^{(k)2}\cos^2\phi_i^{(k)}} \quad 0 \right] \tag{9}$$

and that of $\mathbf{G}_{\boldsymbol{\phi}}^{(k)}$ is

$$\mathbf{G}_{\boldsymbol{\phi}}^{(k)}(i,:) = \left[-\frac{(x^{(k)} - x_i)(z^{(k)} - z_i)}{r_i^{(k)3}\cos\phi_i^{(k)}} \quad -\frac{(y^{(k)} - y_i)(z^{(k)} - z_i)}{r_i^{(k)3}\cos\phi_i^{(k)}} \quad \frac{\cos\phi_i^{(k)}}{r_i^{(k)}} \right] \tag{10}$$

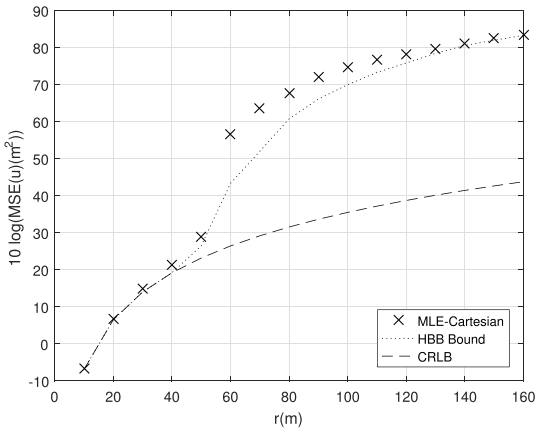

Fig. 2. Thresholding behavior of the source location estimate obtained using AOA measurements in the Cartesian coordinates.

TABLE I
SENSOR POSITIONS FOR 3-D LOCALIZATION, THE UNIT IS METER

i	1	2	3	4	5
x_i	0	-4.64	-4.94	-5.05	-0.28
y_i	0	6.60	-2.13	3.84	5.07
z_i	0	1.55	2.15	1.85	-4.31
i	6	7	8	9	10
x_i	-5.44	-5.40	-5.97	-8.11	-3.46
y_i	7.04	6.63	5.82	-0.28	0.41
z_i	3.10	-5.49	-5.97	-4.08	-4.08

where $r_i^{(k)} = \|\mathbf{u}^{(k)} - \mathbf{s}_i\|$ is the distance between the i-th sensor and intermediate source location estimate.

The iterative expression (7) functions quite well with a good initialization close to the actual solution and yields the CRLB estimation performance, as long as the source is not far away from the sensors and the noise is small. As the range of the source increases, the AOA lines become close to parallel and cannot intersect to yield a point location estimate. This causes the thresholding phenomenon, as illustrated in the simulation shown in Fig. 2. It presents the mean-square error of the source location estimate from the iterative MLE as the source range increases, where its direction is $\theta^o = 101.31°$ and $\phi^o = 30.47°$. The WSN has $M = 10$ sensors and their positions are created randomly as listed in Table I. We assume the azimuth and elevation angles observed by a sensor have the same noise powers and are correlated [33], and the sensors have identical and uncorrelated characteristics. In such a case the covariance matrix $\mathbf{Q}_\mathbf{a}$ is sparse with the diagonal elements equal to $\sigma_\mathbf{a}^2$ and the non-zero off-diagonal elements $\mathbf{Q}_\mathbf{a}(i, M+i) = \mathbf{Q}_\mathbf{a}(M+i, i) = \rho\sigma_\mathbf{a}^2$ for $i = 1, \ldots, M$. In the simulation we set $\sigma_\mathbf{a}^2 = 0.01$ and $\rho = 0.5$. The estimation accuracy is indicated by the mean square error (MSE). The unit of MSE is in m^2 and that of angle noise power is in rad^2. It is clear that when the source range is beyond 50 m, the source location error suddenly becomes very large.

The threshold phenomenon, although the source is not far from the sensors, would also appear when the noise level is large. In this simulation, the noise level is set low enough that the thresholding effect is caused by the increase in the source range.

B. HBB Bound

The CRLB is a widely used lower bound for evaluating the the performance of an estimator because of its computation simplicity. The CRLB is supposed to be applied to an unbiased estimator only, quite often it is used for a biased estimator as well when the bias is negligible compared to variance. One limitation of the CRLB is that it is unable to predict the thresholding effect of a non-linear estimation problem, where the estimation accuracy suddenly becomes very poor as the noise level becoming large or the source moving away from the sensors. To characterize the thresholding behavior for AOA localization, we shall resort to the HBB Bound.

The HBB bound [34] integrates the Bhattacharyya bound [35] and the Hammersley-Chapman-Robbins (HCR) bound [36], [37] together as a single performance bound. The Bhattacharyya bound is a generalization of the CRLB that accounts for the higher order derivatives in the likelihood function. The HCR bound is a simplified version of the Barankin-style bound. The HBB bound yields the CRLB over the small estimation error region. It transits smoothly to the large error region as the noise level or source range increases and produces the HCR bound. The transition between the two regions essentially demonstrates the thresholding behavior of an estimator. The details of the HBB bound evaluation for TDOA localization in Gaussian noise has been illustrated in [31]. The HBB bound for AOA localization follows similar derivations as for TDOA. We shall summarize the main formulas below rather than repeating the derivations for brevity.

The HBB information matrix is [34]

$$\mathbf{H}_{m,l} = \begin{bmatrix} \mathbf{K}_m & \mathbf{L} \\ \mathbf{L}^T & \mathbf{J}_l \end{bmatrix} \tag{11}$$

where m is the order of the Bhattacharyya matrix and l is the number of test points for the HCR bound. We choose $m = 1$ and $l = 4$ in this work to make the computation manageable.

$\mathbf{K}_m$ is the m-th order Bhattacharyya matrix. Let $\boldsymbol{\mu}^o$ be the clean measurement vector parameterized in terms of the source position and $\mathbf{Q}$ the measurement noise covariance matrix. For Gaussian noise,

$$\mathbf{K}_m = \frac{\partial \boldsymbol{\mu}^{oT}}{\partial \mathbf{u}^o} \mathbf{Q}^{-1} \frac{\partial \boldsymbol{\mu}^o}{\partial \mathbf{u}^{oT}}, \tag{12}$$

which is the same as the Fisher Information Matrix (FIM) since we set $m = 1$.

The (i, j)-element of $\mathbf{J}_l$ under the Gaussian noise is [31]

$$\begin{aligned}[\mathbf{J}_l]_{i,j} = \exp\Big\{ \frac{-1}{2} \big[& \boldsymbol{\mu}^{[i]T} \mathbf{Q}^{-1} \boldsymbol{\mu}^{[i]} + \boldsymbol{\mu}^{[j]T} \mathbf{Q}^{-1} \boldsymbol{\mu}^{[j]} \\ & - \boldsymbol{\mu}^{oT} \mathbf{Q}^{-1} \boldsymbol{\mu}^o \\ & - (\boldsymbol{\mu}^{[i]} + \boldsymbol{\mu}^{[j]} - \boldsymbol{\mu}^o)^T \mathbf{Q}^{-1} (\boldsymbol{\mu}^{[i]} + \boldsymbol{\mu}^{[j]} - \boldsymbol{\mu}^o) \big] \Big\}\end{aligned} \tag{13}$$

where $\boldsymbol{\mu}^{[i]}$ is the i-th test point. The k-th block of $\mathbf{L}$ is

$$[\mathbf{L}]_{1,k} = \frac{\partial \boldsymbol{\mu}^{oT}}{\partial \mathbf{u}^o} \mathbf{Q}^{-1} \left(\boldsymbol{\mu}^{[k]} - \boldsymbol{\mu}^o \right). \tag{14}$$

The indices i, j, and k run from 1 to l.

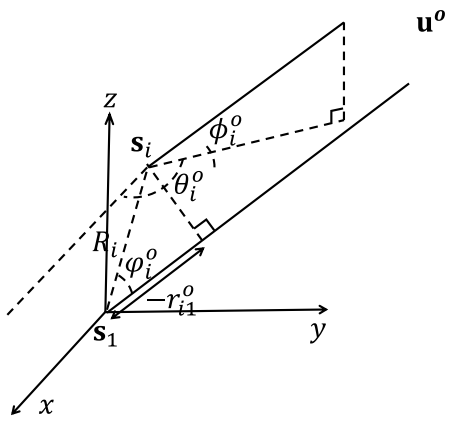

Fig. 3. Far-field localization model.

Let $\boldsymbol{\xi}(\mathbf{u}^o)$ be a transformation of $\mathbf{u}^o$. The HBB bound on the variance of $\boldsymbol{\xi}(\mathbf{u}^o)$ is [34]

$$\operatorname{cov}(\xi) \geqslant \boldsymbol{\Gamma}_{m,l} \mathbf{H}_{m,l}^{-1} \boldsymbol{\Gamma}_{m,l}^T, \tag{15}$$

where

$$\boldsymbol{\Psi}_m = \begin{bmatrix} \dfrac{\partial \boldsymbol{\xi}(\mathbf{u}^o)}{\partial \mathbf{u}^{oT}} & \dfrac{\partial^2 \boldsymbol{\xi}(\mathbf{u}^o)}{\partial \mathbf{u}^{o \otimes 2T}} & \cdots & \dfrac{\partial^m \boldsymbol{\xi}(\mathbf{u}^o)}{\partial \mathbf{u}^{o \otimes mT}} \end{bmatrix} \tag{16}$$

$$\begin{aligned}\boldsymbol{\Phi}_l = [& \boldsymbol{\xi}(\mathbf{u}^{(1)}) - \boldsymbol{\xi}(\mathbf{u}^o) \quad \boldsymbol{\xi}(\mathbf{u}^{(2)}) - \boldsymbol{\xi}(\mathbf{u}^o) \quad \cdots \quad \boldsymbol{\xi}(\mathbf{u}^{(l)}) \\ & - \boldsymbol{\xi}(\mathbf{u}^o)],\end{aligned} \tag{17}$$

$$\boldsymbol{\Gamma}_{m,l} = \begin{bmatrix} \boldsymbol{\Psi}_m & \boldsymbol{\Phi}_l \end{bmatrix}. \tag{18}$$

For AOA measurements, $\boldsymbol{\mu}^o = \mathbf{a}^o$ with the parametric form between the clean measurements and unknown defined in (1) and $\mathbf{Q} = \mathbf{Q}_\mathbf{a}$. The partial derivatives in (12) and (14) are given in Appendix A.

We overlay the HBB bound for the results of the Cartesian MLE in Fig. 2. The HBB bound predicts the thresholding effect very well, which appears when the source range is at around 50.

The HBB bound illustrates it is not possible to estimate the source location in unique coordinates if it is far away from the sensors. A different model than the one of near field as shown in Fig. 1 is needed.

C. Localization in Far-Field

Fig. 3 illustrates the far-field model. The AOA lines from the sensors are all parallel to each other as the wavefront appears linear when the source is in far-field. The AOA lines cannot intersect and we are able to determine only the DOA of the source, which is denoted as $\boldsymbol{\zeta}^o = [\theta^o, \phi^o]^T$. From the data model (2) the cost function of the MLE for DOA localization in the far-field can be written as

$$J_{f,a}(\boldsymbol{\zeta}) = (\mathbf{a} - \boldsymbol{\Lambda}\boldsymbol{\zeta})^T \mathbf{Q}_\mathbf{a}^{-1} (\mathbf{a} - \boldsymbol{\Lambda}\boldsymbol{\zeta}) \tag{19}$$

where $\boldsymbol{\Lambda} = \begin{bmatrix} \mathbf{1} & \mathbf{0} \\ \mathbf{0} & \mathbf{1} \end{bmatrix}$, and $\mathbf{1}$ and $\mathbf{0}$ are $M \times 1$.

$J_{f,a}(\boldsymbol{\zeta})$ is quadratic in the unknown and the solution is

$$\boldsymbol{\zeta} = (\boldsymbol{\Lambda}^T \mathbf{W} \boldsymbol{\Lambda})^{-1} \boldsymbol{\Lambda}^T \mathbf{W} \mathbf{a}, \tag{20}$$

where $\mathbf{W} = \mathbf{Q}_\mathbf{a}^{-1}$.

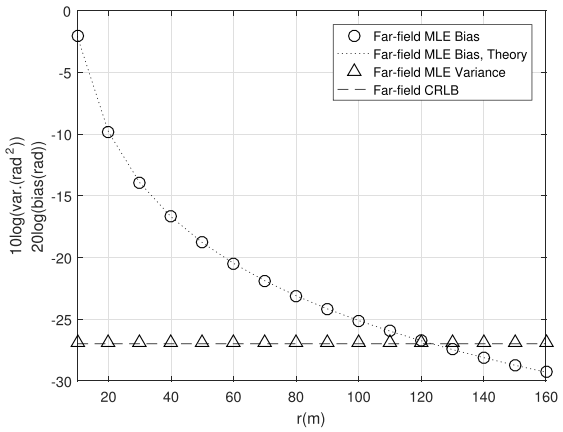

Fig. 4. Bias behaviors of DOA estimates when using the far-field model.

D. DOA Bias

Far-field model eliminates the thresholding effect for a distant source and locates it in DOA. When the source range is not large enough, the far-field model is not able to represent the relationship between the measurements and unknown precisely. Applying the far-field model will result in a large amount of DOA bias as the DOA lines are not nearly parallel.

The theoretical bias can be obtained directly from (20). Subtracting both sides by $\boldsymbol{\zeta}^o$ and taking expectation over the random measurement noise, we arrive at

$$E\left[\boldsymbol{\zeta}-\boldsymbol{\zeta}^o\right]=(\boldsymbol{\Lambda}^T\mathbf{W}\boldsymbol{\Lambda})^{-1}\boldsymbol{\Lambda}^T\mathbf{W}(\mathbf{a}^o-\boldsymbol{\Lambda}\boldsymbol{\zeta}^o). \tag{21}$$

Fig. 4 is the simulation result for the far-field model using the same settings as in Fig. 2. The estimation variance using the far-field model does not exhibit the thresholding effect and shows a constant behavior as the source range increases. It matches well with the CRLB under the far-field model with parallel AOA lines. The bias, on the other hand, is quite significant, especially when the source range is small. The performance of the far-field model is dominated by the bias, when the range is less than 120 in this simulation. The amount of bias from theory (21) predicts the simulation results well.

IV. MPR for AOA Positioning

It appears the thresholding behavior in point positioning with the near-field model is resulted from the range estimate. A large range causes the AOA lines nearly parallel and failing to intersect. The DOA information is inherent in the AOA measurements and the source angle estimates are expected to remain reasonable even if the AOA lines do not intersect. Taking the above into consideration, we propose to estimate the inverse-range instead of range.

The proposed MPR represents the source location by

$$\tilde{\mathbf{u}}^o=\begin{bmatrix}\theta^o & \phi^o & g^o\end{bmatrix}^T, \tag{22}$$

where the first two components are the source azimuth and elevation angles, and g^o is the inverse of the source range, i.e. $g^o=\frac{1}{r^o}$. When the source is in near-field, the inverse-range estimate is significant and the source location $\mathbf{u}^o$ in the Catesian coordinates is obtained from $\tilde{\mathbf{u}}^o$ through the relationship

$$\mathbf{u}^o=(1/g^o)\begin{bmatrix}\cos\theta^o\cos\phi^o & \sin\theta^o\cos\phi^o & \sin\phi^o\end{bmatrix}^T. \tag{23}$$

As the source range increases, g^o as well as its variance approach zero. Consequently, the estimation for $\tilde{\mathbf{u}}^o$ remains stable. Although the inverse-range estimate has no meaning when the source is in far-field, the $\tilde{\mathbf{u}}^o$ estimate will provide the DOA of the source.

We shall derive the Gauss-Newton MLE in MPR below. The HBB bound in MPR will be examined to support the absence of the thresholding effect as the source range increases.

A. MLE in MPR

The MLE in MPR contains two parts. First, we shall propose a Gauss-Newton iterative solution. Second, an SDR method is derived to supply an initial solution to start the iteration.

The ML cost function for optimization is the same as (6), the only difference is to parameterize the unknown as $\tilde{\mathbf{u}}$:

$$J_{n,a}(\tilde{\mathbf{u}})=(\mathbf{a}-\tilde{\mathbf{a}}(\tilde{\mathbf{u}}))^T\,\mathbf{Q}_{\mathbf{a}}^{-1}\,(\mathbf{a}-\tilde{\mathbf{a}}(\tilde{\mathbf{u}})). \tag{24}$$

$\tilde{\mathbf{a}}(\tilde{\mathbf{u}})$ represents the parametric form of the clean AOA vector in terms of $\tilde{\mathbf{u}}$. Linearizing it around $\tilde{\mathbf{u}}^{(0)}$, dropping the higher order terms and applying the chain rule give

$$\tilde{\mathbf{a}}(\tilde{\mathbf{u}})=\tilde{\mathbf{a}}(\tilde{\mathbf{u}}^{(0)})+\frac{\partial\tilde{\mathbf{a}}}{\partial\mathbf{u}^T}\frac{\partial\mathbf{u}}{\partial\tilde{\mathbf{u}}^T}(\tilde{\mathbf{u}}-\tilde{\mathbf{u}}^{(0)}). \tag{25}$$

Using it in (24), taking derivatives and setting the result to zero yield the Gauss-Newton iterative equation

$$\tilde{\mathbf{u}}^{(k+1)}=\tilde{\mathbf{u}}^{(k)}+\mathbf{P}^{(k)}(\mathbf{G}_{\mathbf{a}}^{(k)T}\mathbf{W}\mathbf{G}_{\mathbf{a}}^{(k)})^{-1}\mathbf{G}_{\mathbf{a}}^{(k)T}\mathbf{W}(\mathbf{a}-\tilde{\mathbf{a}}^{(k)}).\quad k=0,1,\ldots \tag{26}$$

In (26),

$$\mathbf{P}^{(k)}=\left(\frac{\partial\mathbf{u}}{\partial\tilde{\mathbf{u}}^T}\bigg|_{\tilde{\mathbf{u}}^{(k)}}\right)^{-1}=\frac{\partial\tilde{\mathbf{u}}}{\partial\mathbf{u}^T}\bigg|_{\tilde{\mathbf{u}}^{(k)}}, \tag{27}$$

$\mathbf{G}_{\mathbf{a}}^{(k)}$ is defined in (8), $\mathbf{W}=\mathbf{Q}_{\mathbf{a}}^{-1}$, $\tilde{\mathbf{a}}^{(k)}$ is the azimuth and elevation angle vector constructed from the $\tilde{\mathbf{u}}^{(k)}$, and $\tilde{\mathbf{u}}^{(0)}$ is the initial solution obtained from SDR which we will elaborate later.

It appears the adjustment term is the same as that for $\mathbf{u}$ in (7), except now we have the additional matrix $\mathbf{P}^{(k)}$. It should be noted that we cannot directly apply (8), it would involve converting $\tilde{\mathbf{u}}^{(k)}$ to $\mathbf{u}^{(k)}$ through (23) as indicated by (9) and (10). (23) is appropriate for near-field source only. When the source is in far-field, $1/g^{(k)}$ is meaningless and the so does $\mathbf{u}^{(k)}$. All of the update variables will need to be in terms of $\tilde{\mathbf{u}}^{(k)}$ only, which are derived as follows.

From (23) and after some algebra, we obtain (28)–(29), as shown at the top of the next page.

To obtain $\mathbf{G}_{\mathbf{a}}^{(k)}$ directly from $\tilde{\mathbf{u}}^{(k)}$, let us define the vector

$$\boldsymbol{\rho}_i^{(k)}=\frac{(\mathbf{u}^{(k)}-\mathbf{s}_i)}{r^{(k)}}=g^{(k)}(\mathbf{u}^{(k)}-\mathbf{s}_i)=\begin{bmatrix}\cos\phi^{(k)}\cos\theta^{(k)}-g^{(k)}x_i\\ \cos\phi^{(k)}\sin\theta^{(k)}-g^{(k)}y_i\\ \sin\phi^{(k)}-g^{(k)}z_i\end{bmatrix}. \tag{30}$$

$$\mathbf{P}^{(k)} = \frac{\partial \tilde{\mathbf{u}}^{(k)}}{\partial \mathbf{u}^{(k)T}} = g^{(k)} \tilde{\mathbf{P}}^{(k)}, \tag{28}$$

$$\tilde{\mathbf{P}}^{(k)} = -\frac{1}{\cos\phi^{(k)}} \begin{bmatrix} \sin\theta^{(k)} & -\cos\theta^{(k)} & 0 \\ \cos\theta^{(k)} \sin\phi^{(k)} \cos\phi^{(k)} & \sin\theta^{(k)} \sin\phi^{(k)} \cos\phi^{(k)} & -\cos^2\phi^{(k)} \\ g^{(k)} \cos\theta^{(k)} \cos^2\phi^{(k)} & g^{(k)} \sin\theta^{(k)} \cos^2\phi^{(k)} & g^{(k)} \sin\phi^{(k)} \cos\phi^{(k)} \end{bmatrix}. \tag{29}$$

$$\mathbf{\Psi}_m = \frac{\partial \boldsymbol{\xi}(\mathbf{u}^o)}{\partial \mathbf{u}^{oT}} = \left(\frac{-1}{r^{o2}\cos\phi^o}\right) \begin{bmatrix} r^o \sin\theta^o & -r^o \cos\theta^o & 0 \\ r^o \cos\theta^o \sin\phi^o cos\phi^o & r^o \sin\theta^o \sin\phi^o \cos\phi^o & -r^o \cos^2\phi^o \\ \cos\theta^o \cos^2\phi^o & \sin\theta^o \cos^2\phi^o & \sin\phi^o \cos\phi^o \end{bmatrix}. \tag{37}$$

Taking the 2-norm on both sides in the first equality of (30), the distance from the i-th sensor to the source estimate after k iterations is

$$r_i^{(k)} = \frac{1}{g^{(k)}} \|\boldsymbol{\rho}_i^{(k)}\|. \tag{31}$$

From (9) and (10), we can express (8) as

$$\mathbf{G}_{\mathbf{a}}^{(k)} = g^{(k)} \tilde{\mathbf{G}}_{\mathbf{a}}^{(k)} = g^{(k)} [\tilde{\mathbf{G}}_{\boldsymbol{\theta}}^{(k)T}, \tilde{\mathbf{G}}_{\boldsymbol{\phi}}^{(k)T}]^T \tag{32}$$

where the rows of $\tilde{\mathbf{G}}_{\boldsymbol{\theta}}^{(k)}$ and $\tilde{\mathbf{G}}_{\boldsymbol{\phi}}^{(k)}$ are

$$\tilde{\mathbf{G}}_{\boldsymbol{\theta}}^{(k)}(i,:) = \frac{\left[-\rho_i^{(k)}(2) \quad \rho_i^{(k)}(1) \quad 0\right]}{\|\boldsymbol{\rho}_i^{(k)}\|^2 \cos^2\phi_i^{(k)}} \tag{33}$$

and

$$\tilde{\mathbf{G}}_{\boldsymbol{\phi}}^{(k)}(i,:) = \frac{\left[-\rho_i^{(k)}(1)\rho_i^{(k)}(3) \quad -\rho_i^{(k)}(2)\rho_i^{(k)}(3) \quad \|\boldsymbol{\rho}_i^{(k)}\|^2 \cos^2\phi_i^{(k)}\right]}{\|\boldsymbol{\rho}_i^{(k)}\|^3 \cos\phi_i^{(k)}}. \tag{34}$$

Finally, it is direct to validate from (1) that the elements of $\tilde{\mathbf{a}}^{(k)}$ can be obtained using

$$\theta_i^{(k)} = \tan^{-1}\left(\frac{\rho_i^{(k)}(2)}{\rho_i^{(k)}(1)}\right),$$
$$\phi_i^{(k)} = \tan^{-1}\left(\frac{\rho_i^{(k)}(3)}{\|\boldsymbol{\rho}_i^{(k)}(1:2)\|}\right). \tag{35}$$

The elements of $\boldsymbol{\rho}_i^{(k)}$ in (33)-(35) are obtained from the last equality in (30).

The update equation (26) now becomes

$$\tilde{\mathbf{u}}^{(k+1)} = \tilde{\mathbf{u}}^{(k)} + \tilde{\mathbf{P}}^{(k)} (\tilde{\mathbf{G}}_{\mathbf{a}}^{(k)T} \mathbf{W} \tilde{\mathbf{G}}_{\mathbf{a}}^{(k)})^{-1} \tilde{\mathbf{G}}_{\mathbf{a}}^{(k)T} \mathbf{W} (\mathbf{a} - \tilde{\mathbf{a}}^{(k)}), \quad k = 0, 1, \ldots \tag{36}$$

It is completely in terms of $\tilde{\mathbf{u}}^{(k)}$ without requiring the inverse of $g^{(k)}$ or the conversion to $\mathbf{u}^{(k)}$.

B. HBB Bound in MPR

The HBB bound on the variance of $\boldsymbol{\xi}(\mathbf{u}) = \tilde{\mathbf{u}}$ is given by (15). All expressions related to the HBB bound in Section III.B remains valid for MPR, the only difference is the variable $\mathbf{\Psi}_m$. With $m = 1$ and using (23), we obtain (37), as shown at the top of this page.

The results presented in section VI validates that the HBB bound for the proposed MPR does not have the thresholding effect in estimating $\tilde{\mathbf{u}}^o$ with respect to the source range. The intuition is that as the range increases, g^o tends to zero which stabilizes the estimate.

C. SDR Solution

The iterative MLE requires an initial solution close to the actual to begin the iteration. To obtain a good initial guess, we begin by exploiting the localization problem with some algebraic manipulations to the AOA measurement equations. Considering the i-th azimuth and elevation angle measurements with the true values expressed in (1),

$$\frac{\eta_{\theta i}}{g^o} \approx \sin\theta_i \left(x^o - x_i\right) - \cos\theta_i \left(y^o - y_i\right)$$
$$\frac{\eta_{\phi i}}{g^o} \approx \cos\theta_i \sin\phi_i \left(x^o - x_i\right) + \sin\theta_i \sin\phi_i \left(y^o - y_i\right) - \cos\phi_i \left(z^o - z_i\right). \tag{38}$$

We have assumed that the measurement noise is small so that $\cos(n_{\theta i}) \approx \cos(n_{\phi i}) \approx 1$, $\sin(n_{\theta i}) \approx n_{\theta i}$ and $\sin(n_{\phi i}) \approx n_{\phi i}$. The residuals resulted from noise are defined as

$$\eta_{\theta i} = \|\boldsymbol{\rho}_i^o(1:2)\| n_{\theta i}$$
$$\eta_{\phi i} = \|\boldsymbol{\rho}_i^o\| n_{\phi i} \tag{39}$$

where

$$\boldsymbol{\rho}_i^o = g^o (\mathbf{u}^o - \mathbf{s}_i)^T \tag{40}$$

$n_{\theta i}$ and $n_{\phi i}$ are the elements of the AOA noise vector $\mathbf{n_a}$ for sensor i. Multiplying by g^o on both sides and ignoring the approximation errors, (38) becomes

$$\eta_{\theta i} = \sin\theta_i \cos\theta^o \cos\phi^o - \cos\theta_i \sin\theta^o \cos\phi^o - g^o (x_i \sin\theta_i - y_i \cos\theta_i)$$
$$\eta_{\phi i} = \cos\theta_i \sin\phi_i \cos\theta^o \cos\phi^o + \sin\theta_i \sin\phi_i \sin\theta^o \cos\phi^o - \cos\phi_i \sin\phi^o - g^o (x_i \cos\theta_i \sin\phi_i + y_i \sin\theta_i \sin\phi_i - z_i \cos\phi_i). \tag{41}$$

We arrive at two equations where the unknowns are θ^o, ϕ^o and g^o. They are coupled together and difficult to obtain. Rather than solving them directly, we introduce additional variables, impose constraints on them and solve the constrained optimization problem by the convex optimization through semidefinite relaxation.

Stacking the $2M$ equations of (41) over i from 1 to M yields

$$\mathbf{B_a} \mathbf{n_a} = \mathbf{A_a} \mathbf{v}^o. \tag{42}$$

The unknown vector is

$$\mathbf{v}^o = \left[\cos\theta^o \cos\phi^o \quad \sin\theta^o \cos\phi^o \quad \sin\phi^o \quad g^o\right]^T. \quad (43)$$

The $2M \times 4$ matrix

$$\mathbf{A_a} = [\mathbf{A}_{\boldsymbol{\theta}}^T, \mathbf{A}_{\boldsymbol{\phi}}^T]^T \quad (44)$$

is known. The i-th rows of $\mathbf{A}_{\boldsymbol{\theta}}$ and $\mathbf{A}_{\boldsymbol{\phi}}$ are

$$\begin{aligned}\mathbf{A}_{\boldsymbol{\theta}}(i,:) &= \left[\sin\theta_i \quad -\cos\theta_i \quad 0 \quad -(x_i\sin\theta_i - y_i\cos\theta_i)\right],\\ \mathbf{A}_{\boldsymbol{\phi}}(i,:) &= [\cos\theta_i\sin\phi_i \quad \sin\theta_i\sin\phi_i \quad -\cos\phi_i\\ &\quad -(x_i\cos\theta_i\sin\phi_i + y_i\sin\theta_i\sin\phi_i - z_i\cos\phi_i)].\end{aligned} \quad (45)$$

On the left side, the $2M \times 2M$ diagonal matrix $\mathbf{B_a}$ is given by

$$\begin{aligned}\mathbf{B_a} &= \mathrm{diag}(\mathbf{B}_{\boldsymbol{\theta}}, \mathbf{B}_{\boldsymbol{\phi}}),\\ \mathbf{B}_{\boldsymbol{\theta}} &= \mathrm{diag}([\|\boldsymbol{\rho}_1^o(1:2)\|, \ldots, \|\boldsymbol{\rho}_M^o(1:2)\|]),\\ \mathbf{B}_{\boldsymbol{\phi}} &= \mathrm{diag}([\|\boldsymbol{\rho}_1^o\|, \ldots, \|\boldsymbol{\rho}_M^o\|]).\end{aligned} \quad (46)$$

The elements in $\mathbf{v}^o$ are dependent. According to (42) and (43), the solution is

$$\mathbf{v} = \underset{\mathbf{v}}{\mathrm{argmin}}\ \mathbf{v}^T\mathbf{A}_{\mathbf{a}}^T\mathbf{W_a}\mathbf{A_a}\mathbf{v} \quad (47)$$

subject to

$$1 = \upsilon(1)^2 + \upsilon(2)^2 + \upsilon(3)^2. \quad (48)$$

$\mathbf{W_a} = \left(\mathbf{B_a}\mathbf{Q_a}\mathbf{B}_{\mathbf{a}}^T\right)^{-1}$ is the weighting matrix. (47) is a weighted least squares optimization problem with a quadratic constraint. It can be solved by applying the SDR technique.

We shall obtain $\mathbf{V} = \mathbf{v}\mathbf{v}^T$ instead by relaxing its rank to be larger than one. In doing so, the problem described in (47) and (48) is expressed as

$$\mathbf{V} = \underset{\mathbf{V}\in S^4}{\mathrm{argmin}}\ \mathrm{tr}\left(\mathbf{A}_{\mathbf{a}}^{\mathrm{T}}\mathbf{W_a}\mathbf{A_a}\mathbf{V}\right) \quad (49)$$

subject to

$$\begin{aligned}0 &= 1 - \mathrm{tr}\,(\mathbf{MV})\\ \mathbf{V} &\succeq 0\end{aligned} \quad (50)$$

where

$$\mathbf{M} = \begin{bmatrix}1 & 0 & 0 & 0\\ 0 & 1 & 0 & 0\\ 0 & 0 & 1 & 0\\ 0 & 0 & 0 & 0\end{bmatrix}. \quad (51)$$

(49) can be solved using a convex optimization package such as CVX. The solution of $\mathbf{v}$ is

$$\mathbf{v} = \sqrt{\lambda_{max}}\mathbf{v}_{max}, \quad (52)$$

where $\mathbf{v}_{max}$ is the eigenvector of $\mathbf{V}$ having the largest eigenvalue λ_{max}. From the definition of $\mathbf{v}^o$ in (43), the initial solution to start the MLE is

$$\begin{aligned}\tilde{\mathbf{u}}^{(0)} &= [\tan^{-1}(\upsilon(2)/\upsilon(1))\\ &\qquad \tan^{-1}\left(\upsilon(3)/\sqrt{\upsilon(1)^2+\upsilon(2)^2}\right) \quad \upsilon(4)]^T.\end{aligned} \quad (53)$$

Note that $\mathbf{B_a}$ in the weighting matrix depends on the true value of the solution. As a common approach [38], we set $\mathbf{W_a}$ to an identity matrix to obtain a preliminary solution, which is essentially the least-squares solution instead of the weighted least-squares. An approximate of the weighting matrix can be generated from the preliminary solution and a better estimate can be obtained. The process can repeat a few times to improve the results. Simulations indicate that repeating once or twice is sufficient.

V. Proposed MPR for Hybrid AOA and TDOA

[31] introduced MPR for TDOA measurements. In this section, we consider MPR for a hybrid system that utilizes both the AOA and TDOA measurements for positioning. The motivation is to exploit the additional measurements for improving the localization accuracy or reducing the number of sensors used.

The measurement model is (5) in this case. The MLE is the solution that minimizes

$$J_n = (\mathbf{m} - \tilde{\mathbf{m}})^T\,\mathbf{Q}_{\mathbf{m}}^{-1}\,(\mathbf{m} - \tilde{\mathbf{m}}) \quad (54)$$

where $\tilde{\mathbf{m}}$ represents the parametric form of the clean measurement vector parameterized in terms of $\mathbf{u}$ for the Cartesian MLE or $\tilde{\mathbf{u}}$ for the MPR MLE.

We shall first summarize briefly the HBB bound for hybrid AOA-TDOA positioning. The DOA bias from the far-field model is derived. We next present the proposed MLE in MPR for hybrid positioning, and finally develop the SDR solution for initializing the iterative MLE.

A. HBB Bound

The HBB bound presented in Section III.B will be valid for the hybrid model after re-defining some variables. The clean measurement vector is $\boldsymbol{\mu}^o = \mathbf{m}^o$, where the parametric form is described in (1) and (3). The partial derivatives in (12) and (14) are given in Appendix A. For the Cartesian representation, $\boldsymbol{\xi}(\mathbf{u}^o) = \mathbf{u}^o$ and $\boldsymbol{\Psi}_m$ is an identity matrix of size 3. For MPR, $\boldsymbol{\xi}(\mathbf{u}) = \tilde{\mathbf{u}}$ and $\boldsymbol{\Psi}_m$ is given by (37).

B. DOA Bias

The AOA and TDOA measurements are uncorrelated according to the problem formulation in Section II. As a result, under the far-field model the cost function to be minimized for DOA estimation is

$$J_f = J_{f,a} + J_{f,r}. \quad (55)$$

$J_{f,a}$ is the component from AOA and is defined in (19) or (89). $J_{f,r}$ is the component from TDOA. According to the far-field model as illustrated in Fig. 3,

$$-r_{i1}^o = R_i\cos\varphi_i^o \quad (56)$$

where R_i is the Euclidean distance between sensors $\mathbf{s}_i$ and $\mathbf{s}_1$, and φ_i^o is the angle at $\mathbf{s}_1$ subtended by $\mathbf{s}_i$ and $\mathbf{u}^o$. We have from (4),

$$\begin{aligned}J_{f,r} &= (\mathbf{r} - \tilde{\mathbf{r}})^T\mathbf{Q}_{\mathbf{r}}^{-1}(\mathbf{r} - \tilde{\mathbf{r}})\\ &= \sum_{i,j=2}^{M} w_{2M+i-1,2M+j-1}(r_{i1} + R_i\cos\varphi_i)(r_{j1} + R_j\cos\varphi_j),\end{aligned} \quad (57)$$

where $w_{i,j}$ is the (i, j)-th element of $\mathbf{Q}_\mathbf{m}^{-1}$. Through the dot product relationship between the two vectors $\mathbf{s}_i - \mathbf{s}_1$ and $\mathbf{u} - \mathbf{s}_1$, the angle φ_i is related to the source DOA $\boldsymbol{\zeta}$ by

$$\begin{aligned}\cos\varphi_i &= \cos\alpha_i \cos\theta \cos\beta_i \cos\phi \\ &\quad + \sin\alpha_i \sin\theta \cos\beta_i \cos\phi + \sin\beta_i \sin\phi. \end{aligned} \tag{58}$$

The DOA bias is derived using the fact that the gradient of J_f is zero at the solution, i.e. $\mathbf{J}'_f(\boldsymbol{\zeta}) = 0$, where the superscript "$'$" represents derivative with respect to the variable. Expanding $\mathbf{J}'_f(\boldsymbol{\zeta})$ through the Taylor-series at the true value $\boldsymbol{\zeta}^o$ and neglecting the second and higher order terms, the bias is

$$E\left[\boldsymbol{\zeta} - \boldsymbol{\zeta}^o\right] = -E\left[\mathbf{J}''_f(\boldsymbol{\zeta}^o)^{-1}\mathbf{J}'_f(\boldsymbol{\zeta}^o)\right]. \tag{59}$$

In the above expression $\boldsymbol{\zeta}$ is considered as the minimizer of J_f. The measurements are noisy and

$$\mathbf{J}'_f(\boldsymbol{\zeta}^o) = \bar{\mathbf{J}}'_f(\boldsymbol{\zeta}^o) + \Delta\mathbf{J}'_f(\boldsymbol{\zeta}^o), \tag{60}$$

where $\bar{\mathbf{J}}'_f(\boldsymbol{\zeta}^o)$ is the expected value without noise and $\Delta\mathbf{J}'_f(\boldsymbol{\zeta}^o)$ is the component resulting from random noise. Note that $E[\Delta\mathbf{J}'_f(\boldsymbol{\zeta}^o)] = 0$. Similarly,

$$\mathbf{J}''_f(\boldsymbol{\zeta}^o) = \bar{\mathbf{J}}''_f(\boldsymbol{\zeta}^o) + \Delta\mathbf{J}''_f(\boldsymbol{\zeta}^o) \tag{61}$$

and $E[\Delta\mathbf{J}''_f(\boldsymbol{\zeta}^o)] = 0$. Substituting (60) and (61) into (59) and applying matrix inverse approximation, (59) becomes

$$E\left[\boldsymbol{\zeta} - \boldsymbol{\zeta}^o\right] = -\bar{\mathbf{J}}''^{-1}_f\bar{\mathbf{J}}'_f + (\bar{\mathbf{J}}''^T_f\bar{\mathbf{J}}''_f)^{-1}E\left[\Delta\mathbf{J}''^T_f\Delta\mathbf{J}'_f\right]. \tag{62}$$

The bias has two components, one is from the far-field modeling defined by the first term and the other from noise defined in the second term. Appendix B provides the details for the various terms in (62) from which the bias can be evaluated.

C. MLE in MPR

The resulting MLE in MPR is a concatenation of those for the AOA and TDOA. The Gauss-Newton iterative equation is

$$\begin{aligned}\tilde{\mathbf{u}}^{(k+1)} &= \tilde{\mathbf{u}}^{(k)} + \tilde{\mathbf{P}}^{(k)}(\mathbf{G}^{(k)T}\mathbf{W}\mathbf{G}^{(k)})^{-1}\mathbf{G}^{(k)T}\mathbf{W}(g^{(k)}\mathbf{m} - \tilde{\mathbf{m}}^{(k)}), \\ &\quad k = 0, 1, \ldots \end{aligned} \tag{63}$$

where $\mathbf{W} = \mathbf{Q}_\mathbf{m}^{-1}$. The iteration starts with an initial solution $\tilde{\mathbf{u}}^{(0)}$ and k is the update count. All variables in (63) are in terms of $\tilde{\mathbf{u}}^{(k)}$ without requiring the evaluation of $1/g^{(k)}$ or the conversion to $\mathbf{u}^{(k)}$. Specifically, $\tilde{\mathbf{P}}^{(k)}$ is given in (29). The matrix $\mathbf{G}^{(k)} = [\mathbf{G}_\mathbf{a}^{(k)T}, \mathbf{G}_\mathbf{r}^{(k)T}]^T$ consists of the Jocobians of the AOA and TDOA measurements. $\mathbf{G}_\mathbf{a}^{(k)}$ is defined in (32) and from [31]

$$\mathbf{G}_\mathbf{r}^{(k)}(i-1, :) = \left(\frac{\boldsymbol{\rho}_i^{(k)}}{\|\boldsymbol{\rho}_i^{(k)}\|} - \frac{\boldsymbol{\rho}_1^{(k)}}{\|\boldsymbol{\rho}_1^{(k)}\|}\right)^T \tag{64}$$

where $\boldsymbol{\rho}_i{}^{(k)}$ is defined in (30) and i runs from 2 to M. The constructed measurement vector is

$$\tilde{\mathbf{m}}^{(k)} = [g^{(k)}\tilde{\mathbf{a}}^{(k)T}, \quad \tilde{\mathbf{r}}^{(k)T}]^T. \tag{65}$$

$\tilde{\mathbf{a}}^{(k)}$ is obtained through (35). The elements of $\tilde{\mathbf{r}}^{(k)}$ are [31]

$$\tilde{r}_{i1}^{(k)} = \|\boldsymbol{\rho}_i^{(k)}\| - \|\boldsymbol{\rho}_1^{(k)}\|, \quad i = 2, 3, \cdots, M. \tag{66}$$

D. Initial Solution

Using a geometric approach we can obtain a set of algebraic equations for the TDOA measurements, as shown in (29) of [31]. The algebraic equations for AOA are given in (42). Cascading them together yields

$$\mathbf{B}\mathbf{n} = \mathbf{m} - \mathbf{A}\mathbf{v}^o. \tag{67}$$

In (67), the unknown vector $\mathbf{v}^o$ is defined as

$$\begin{aligned}\mathbf{v}^o = [&\cos\theta^o\cos\phi^o \quad \sin\theta^o\cos\phi^o \quad \sin\phi^o \quad g^o\cos^2\theta^o\cos^2\phi^o \\ &g^o\sin^2\theta^o\cos^2\phi^o \quad g^o\sin^2\phi^o \quad g^o\sin\theta^o\cos\theta^o\cos^2\phi^o \\ &g^o\cos\theta^o\sin\phi^o\cos\phi^o \quad g^o\sin\theta^o\sin\phi^o\cos\phi^o]^T. \end{aligned} \tag{68}$$

$\mathbf{A} = [\mathbf{A}_\mathbf{a}^T, \mathbf{A}_\mathbf{r}^T]^T$ is a $(3M-1)\times 9$ matrix. $\mathbf{A}_\mathbf{a}$ is given in (44) and from (41) for $i = 1, 2, \cdots, M$

$$\begin{aligned}&\mathbf{A}_{\boldsymbol{\theta}}(i, :) \\ &= [\sin\theta_i \quad -\cos\theta_i \quad 0 \quad -(x_i\sin\theta_i - y_i\cos\theta_i) \\ &\quad -(x_i\sin\theta_i - y_i\cos\theta_i) \quad -(x_i\sin\theta_i - y_i\cos\theta_i) \quad 0 \quad 0 \quad 0], \end{aligned} \tag{69}$$

$$\begin{aligned}&\mathbf{A}_{\boldsymbol{\phi}}(i, :) \\ &= [\cos\theta_i\sin\phi_i \quad \sin\theta_i\sin\phi_i \quad -\cos\phi_i \\ &\quad -(x_i\cos\theta_i\sin\phi_i + y_i\sin\theta_i\sin\phi_i - z_i\cos\phi_i) \\ &\quad -(x_i\cos\theta_i\sin\phi_i + y_i\sin\theta_i\sin\phi_i - z_i\cos\phi_i) \\ &\quad -(x_i\cos\theta_i\sin\phi_i + y_i\sin\theta_i\sin\phi_i - z_i\cos\phi_i) \quad 0 \quad 0 \quad 0]. \end{aligned} \tag{70}$$

Regarding the TDOA portion, the $(i-1)$-th row of $\mathbf{A}_\mathbf{r}$, $i = 2, 3, \cdots, M$, is [31]

$$\begin{aligned}&\mathbf{A}_\mathbf{r}(i-1, :) \\ &\quad = [-R_i\cos\alpha_i\cos\beta_i \quad -R_i\sin\alpha_i\cos\beta_i \quad -R_i\sin\beta_i \\ &\quad \frac{R_i^2(1-\cos\alpha_i{}^2\cos\beta_i{}^2)}{2} \quad \frac{R_i^2(1-\sin\alpha_i{}^2\cos\beta_i{}^2)}{2} \\ &\quad \frac{R_i^2\cos\beta_i{}^2}{2} \quad -R_i^2\sin\alpha_i\cos\alpha_i\cos\beta_i{}^2 \\ &\quad -R_i^2\cos\alpha_i\sin\beta_i\cos\beta_i - R_i^2\sin\alpha_i\sin\beta_i\cos\beta_i]. \end{aligned} \tag{71}$$

The $3M\times 3M$ matrix $\mathbf{B}$ is block-diagonal given by

$$\mathbf{B} = \mathrm{diag}(\mathbf{B}_\mathbf{a}, \mathbf{I}) \tag{72}$$

where $\mathbf{B}_\mathbf{a}$ is defined in (46) and $\mathbf{I}$ of of size $M-1$. The elements of $\mathbf{v}^o$ are not independent and their relationships are exploited through constraints.

We obtain $\mathbf{v}$ by solving the constrained minimization problem

$$\mathbf{v} = \underset{\mathbf{v}}{\mathrm{argmin}} \ (\mathbf{m} - \mathbf{A}\mathbf{v})^T\mathbf{W}(\mathbf{m} - \mathbf{A}\mathbf{v}) \tag{73}$$

subject to

$$\begin{aligned}1 &= \upsilon(1)^2 + \upsilon(2)^2 + \upsilon(3)^2 \\ 0 &= \upsilon(1)\upsilon(9) - \upsilon(2)\upsilon(8) \\ 0 &= \upsilon(1)\upsilon(9) - \upsilon(3)\upsilon(7) \\ 0 &= \upsilon(1)\upsilon(6) - \upsilon(3)\upsilon(8) \\ 0 &= \upsilon(2)\upsilon(6) - \upsilon(3)\upsilon(9) \\ 0 &= \upsilon(4)\upsilon(5) - \upsilon(7)^2. \end{aligned} \tag{74}$$

From the left side of (67), $\mathbf{W} = (\mathbf{BQ_mB})^{-1}$. It is solved by using $\mathbf{V} = \mathbf{v}\mathbf{v}^T$ as the variable instead and relaxing its rank larger than 1. In such a case, (73)-(74) are re-written as

$$\mathbf{V} = \underset{\mathbf{V}\in S^9}{\operatorname{argmin}} - 2\sqrt{\operatorname{tr}(\mathbf{A}^T\mathbf{W}\mathbf{m}\mathbf{m}^T\mathbf{W}\mathbf{A}\mathbf{V})} + \operatorname{tr}(\mathbf{A}^T\mathbf{W}\mathbf{A}\mathbf{V}) \quad (75)$$

subject to

$$\begin{aligned} 0 &= 1 - \operatorname{tr}(\mathbf{M}_1\mathbf{V}),\\ 0 &= 0 - \operatorname{tr}(\mathbf{M}_2\mathbf{V}),\\ 0 &= 0 - \operatorname{tr}(\mathbf{M}_3\mathbf{V}),\\ 0 &= 0 - \operatorname{tr}(\mathbf{M}_4\mathbf{V}),\\ 0 &= 0 - \operatorname{tr}(\mathbf{M}_5\mathbf{V}),\\ 0 &= 0 - \operatorname{tr}(\mathbf{M}_6\mathbf{V}),\\ \mathbf{V} &\succeq 0. \end{aligned} \quad (76)$$

$\mathbf{M}_i$, $i = 1, \ldots, 6$, are sparse matrices defined as

$$\begin{aligned} &\mathbf{M}_1(1,1) = \mathbf{M}_1(2,2) = \mathbf{M}_1(3,3) = 1,\\ &\mathbf{M}_2(1,9) = \mathbf{M}_2(9,1) = 1, \quad \mathbf{M}_2(2,8) = \mathbf{M}_2(8,2) = -1,\\ &\mathbf{M}_3(1,9) = \mathbf{M}_3(9,1) = 1, \quad \mathbf{M}_3(3,7) = \mathbf{M}_3(7,3) = -1,\\ &\mathbf{M}_4(1,6) = \mathbf{M}_4(6,1) = 1, \quad \mathbf{M}_4(3,8) = \mathbf{M}_4(8,3) = -1,\\ &\mathbf{M}_5(2,6) = \mathbf{M}_5(6,2) = 1, \quad \mathbf{M}_5(3,9) = \mathbf{M}_5(9,3) = -1,\\ &\mathbf{M}_6(4,5) = \mathbf{M}_6(5,4) = 1, \quad \mathbf{M}_6(7,7) = -2. \end{aligned} \quad (77)$$

Let λ_{max} be the largest eigenvalue of the obtained $\mathbf{V}$ solution and $\mathbf{v}_{max}$ the corresponding eigenvector. The solution of $\mathbf{v}$ is (52).

It is noted that $\phi \in [-\pi/2, \pi/2]$. From (68), the initial solution of the hybrid MLE is

$$\tilde{\mathbf{u}}^{(0)} = \left[\tan^{-1}(v(2)/v(1)) \quad \tan^{-1}\left(v(3)/\sqrt{v(1)^2 + v(2)^2}\right) \quad v(4) + v(5) + v(6)\right]^T. \quad (78)$$

In theory two sensors are sufficient to locate the source in hybrid AOA-TDOA positioning [30]. For the proposed SDR solution, extra sensors for additional measurements may be needed due to the rank relaxation.

E. Contribution of TDOA in Reducing the CRLB

We examine the TDOA measurements for improving the positioning accuracy. To simplify the illustration, we assume the AOA and TDOA measurements are uncorrelated.

The FIM [39] for the source location using both AOA and TDOA measurements is

$$\begin{aligned} \mathbf{FIM} &= \mathbf{FIM_a} + \mathbf{FIM_r}\\ &= \frac{\partial \mathbf{a}^T}{\partial \tilde{\mathbf{u}}}\mathbf{Q}_\mathbf{a}^{-1}\frac{\partial \mathbf{a}}{\partial \tilde{\mathbf{u}}^T} + \frac{\partial \mathbf{r}^T}{\partial \tilde{\mathbf{u}}}\mathbf{Q}_\mathbf{r}^{-1}\frac{\partial \mathbf{r}}{\partial \tilde{\mathbf{u}}^T}. \end{aligned} \quad (79)$$

$\mathbf{FIM_a}$ is the FIM using AOA only and $\mathbf{FIM_r}$ using TDOA only. Taking the inverse of $\mathbf{FIM}$ and applying the matrix inversion lemma [39] gives

$$\begin{aligned} \mathbf{CRLB} &= \mathbf{CRLB_a}\\ &\quad - \mathbf{CRLB_a}\frac{\partial \mathbf{r}^T}{\partial \tilde{\mathbf{u}}}\left(\mathbf{Q_r} + \frac{\partial \mathbf{r}}{\partial \tilde{\mathbf{u}}^T}\mathbf{CRLB_a}\frac{\partial \mathbf{r}^T}{\partial \tilde{\mathbf{u}}}\right)^{-1}\\ &\quad \times \frac{\partial \mathbf{r}}{\partial \tilde{\mathbf{u}}^T}\mathbf{CRLB_a} \end{aligned} \quad (80)$$

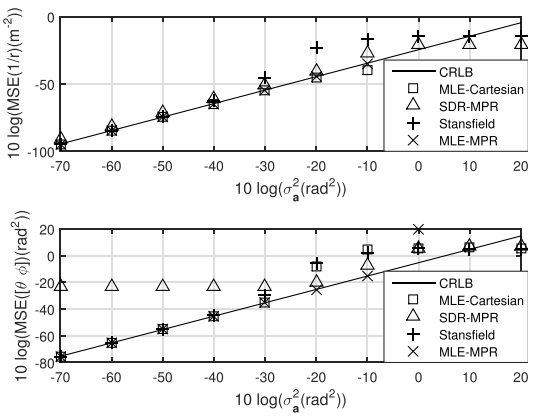

Fig. 5. Performance of the proposed MLE-MPR using AOA measurements.

where $\mathbf{CRLB_a} = \mathbf{FIM_a}^{-1}$ is the CRLB of $\tilde{\mathbf{u}}$ when applying only AOA measurements. According to the second term of (80), adding TDOA measurements always reduces the CRLB and improves the localization performance. The amount of improvement depends on the TDOA accuracy reflected by $\mathbf{Q_r}$ and the localization geometry embedded in the partial derivative.

VI. Simulations

This section examines the performance of the proposed methods for AOA and hybrid AOA-TDOA localizations. We shall denote the proposed algorithm as MLE-MPR, whereas the near-field Gauss-Newton MLE in the Cartesian coordinates as MLE-Cartesian. The proposed initial solution from SDR is labeled by SDR-MPR. We use the same sensor and source geometry as in Fig. 2, which is described after (10). The number of ensemble runs is 1000. The units of angle MSE and angle noise power are both in rad^2. The noise power for TDOA is in m^2.

A. AOA

Before investigating the performance of AOA localization as the source range increases, we evaluate the performance of the proposed MLE-MPR and SDR-MPR at a fixed source range of 80 m but varying the AOA noise power. Also included for comparison is a popular algorithm for AOA localization, the Stansfield algorithm [40], [41]. Fig. 5 indicates MLE-MPR and MLE-Cartesian achieve the CRLB accuracy and outperform SDR-MPR when the noise level is below 0.01. Both the MLE-MPR and SDR-MPR are a little more stable than MLE-Cartesian and the Stansfield algorithm at larger noise level around 0.01 to 0.1. Fig. 6 illustrates the estimation bias. The bias behaviors of the estimators are consistent with those of MSE in Fig. 5. It is the significant amount of bias that SDR-MPR has an MSE above the CRLB at low noise and below at high noise.

We next keep the noise power $\sigma_\mathbf{a}^2$ at 0.01 and increase the source range. Fig. 2 illustrates the thresholding behavior of AOA localization in the Cartesian coordinates. When we apply MLE-MPR to the same simulation, the estimation performance is illustrated in Fig. 7. No thresholding effect appears for

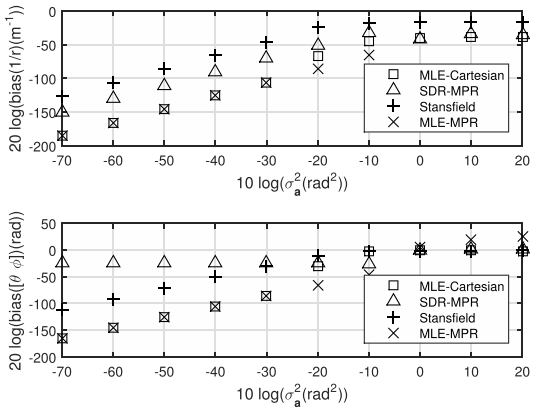

Fig. 6. Bias behavior of the proposed MLE-MPR using AOA measurements.

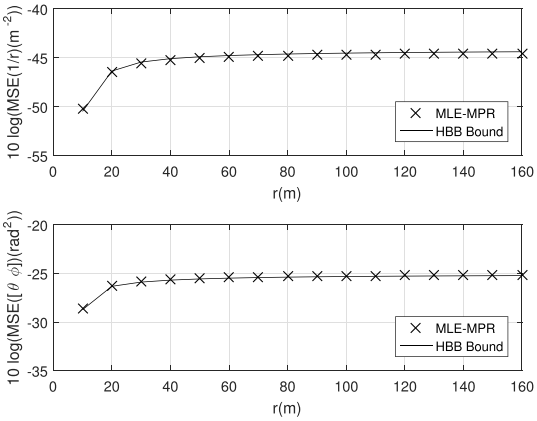

Fig. 7. Performance of the source location estimate using AOA measurements in MPR as the source range increases.

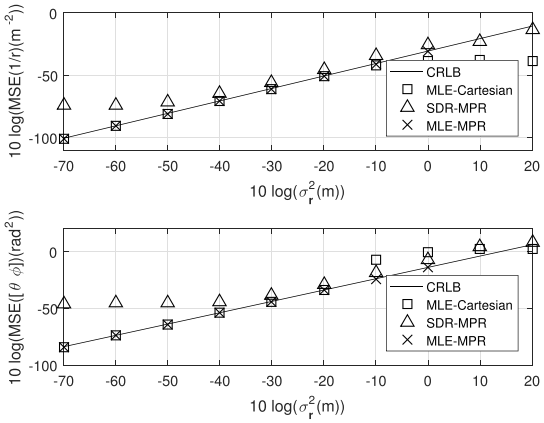

Fig. 8. Performance of the proposed MLE-MPR using hybrid AOA and TDOA measurements.

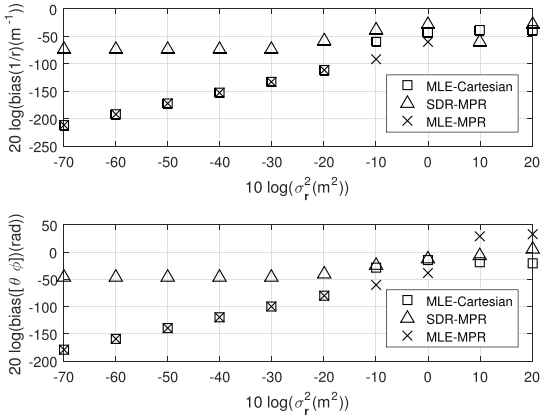

Fig. 9. Bias behavior of the proposed MLE-MPR using hybrid AOA and TDOA measurements.

both the inverse source range and the source direction. In the near-field region where the source range is not large, the inverse range is meaningful and applying (23) yields a unique point position of the source. When the source is too far away, the inverse source range is close to zero and is meaningless. Nevertheless, the source direction estimated by MLE-MPR remains accurate. There is no need to handle near-field source and far-field source separately by switching models.

B. Hybrid AOA and TDOA

Figs. 8 and 9 show the MSE and bias performance of hybrid AOA-TDOA positioning at the source range equal to 80 m. The TDOA covariance matrix is $\mathbf{Q_r} = 0.5\sigma_{\mathbf{r}}^2(\mathbf{I} + \mathbf{1}\mathbf{1}^T)$ [22], where $\sigma_{\mathbf{r}}^2$ is the TDOA noise power and it is identical to the AOA noise power in this simulation. The correlation between the AOA and TDOA measurement noise is zero. The performance of MLE-MPR in Fig. 8 remains consistent in reaching the CRLB when the noise power is not large. It has better performance than MLE-Cartesian and SDR-MPR at the noise power equal to 1. However, when the noise power is larger than 1, the thresholding effect appears and the estimation accuracy of MLE-MPR becomes very poor (MSE value is outside the range of the plot). SDR-MPR does not perform well at low noise level but it is more stable than MLE-MPR and MLE-Cartesian when the noise level is beyond 1. As expected, MLE-MPR has the best bias performance as shown in Fig. 9. The MSE of SDR-MPR in Fig. 8 is dominated by its large amount of bias.

Correlation between AOA and TDOA observations is zero in the results shown for ease of illustration. We have done simulations for non-zero correlation between them as well. The proposed solutions are insensitive to the correlation and MLE-MPR remains to reach the CRLB accuracy when the noise level is not significant. This is because the proposed solutions are based on the ML formulation where the noise correlations are taken into account in the covariance matrix.

Keeping the measurement noise powers at $\sigma_{\mathbf{a}}^2 = 0.01$ and $\sigma_{\mathbf{r}}^2 = 0.01$, we next evaluate the performance of the estimators as the source range increases. Fig. 10 presents the result of MLE-Cartesian. Comparing to Fig. 2 where only AOA is used, the accuracy increases and the performance deviates from the CRLB later at source range equal to 90 m instead of 50 m. Nevertheless, once the thresholding effect occurs, the performance is quite worse. The HBB bound matches the simulation well and predicts accurately the source range where the thresholding behavior occurs.

Fig. 11 illustrates the performance of MLE-MPR. Both the inverse range and direction estimates are quite stable as

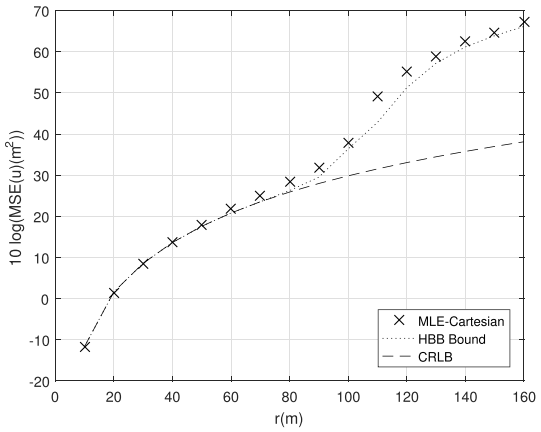

Fig. 10. Thresholding behavior of the source location estimate obtained using hybrid AOA and TDOA measurements in the Cartesian coordinates.

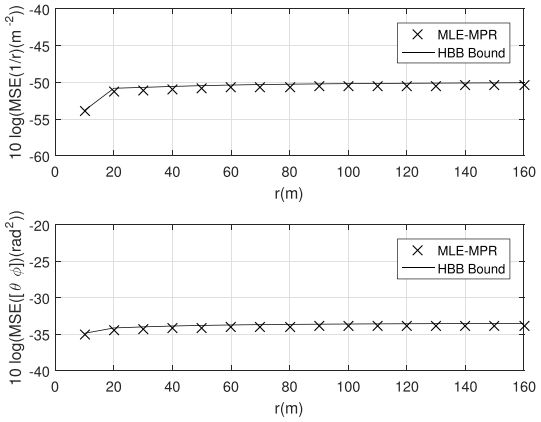

Fig. 11. Performance of the source location estimate using hybrid AOA and TDOA measurements in MPR as the source range increases.

the source range increases. The estimation accuracy improves when comparing to Fig. 7, due to the use of the additional TDOA measurements.

The simulations used equal noise powers for the measurements from different sensors for simplicity. Such assumption may not hold for widely distributed sensors since the measurement noise power from a sensor is typically related to the distance between the source and the sensor. As the source range increases, the noise powers would be close. Nevertheless, the proposed Gauss-Newton based algorithm is based on the ML formulation and it is expected to reach the CRLB performance for any positive definite noise covariance matrix before the thresholding effect occurs. We have made confirmation by repeating Fig. 5 when the noise powers from different sensors are proportional to the square of the distance to the source.

VII. Conclusion

The paper develops a unified approach for AOA localization of a source that can be in near-field or far-field. We first use the HBB bound to illustrate the thresholding behavior in locating a source in a unique position using the near-field model when it becomes distant. The bias in the source DOA estimate is examined when a far-field model is applied instead. MPR is then introduced and an iterative MLE in MPR is developed. A coarse solution obtained from SDR is proposed to initialize the MLE. The HBB bound, the iterative MLE in MPR and the SDR solution are extended for hybrid AOA-TDOA positioning. Simulations verify the theoretical development and the algorithm performance.

Appendix A

To compute the HBB bound for AOA positioning, the partial derivative of the measurement vector is given by

$$\frac{\partial \boldsymbol{\mu}^o}{\partial \mathbf{u}^{oT}} = \frac{\partial \mathbf{a}^o}{\partial \mathbf{u}^{oT}} = \left[\left(\frac{\partial \boldsymbol{\theta}^o}{\partial \mathbf{u}^{oT}} \right)^T \quad \left(\frac{\partial \boldsymbol{\phi}^o}{\partial \mathbf{u}^{oT}} \right)^T \right]^T, \tag{81}$$

where

$$\frac{\partial \theta_i^o}{\partial \mathbf{u}^{oT}} = \left[-\frac{y^o - y_i}{r_i^{o2} \cos^2 \phi_i^o} \quad \frac{x^o - x_i}{r_i^{o2} \cos^2 \phi_i^o} \; 0 \right], \tag{82}$$

$$\frac{\partial \phi_i^o}{\partial \mathbf{u}^{oT}} = \left[-\frac{(x^o - x_i)(z^o - z_i)}{r_i^{o3} \cos \phi_i^o} \quad -\frac{(y^o - y_i)(z^o - z_i)}{r_i^{o3} \cos \phi_i^o} \quad \frac{\cos \phi_i^o}{r_i^o} \right]. \tag{83}$$

$r_i^o = \|\mathbf{u}^o - \mathbf{s}_i\|$ is the distance from the source to the i-th sensor.

For the hybrid AOA-TDOA positioning,

$$\frac{\partial \boldsymbol{\mu}^o}{\partial \mathbf{u}^{oT}} = \frac{\partial \mathbf{m}^o}{\partial \mathbf{u}^{oT}} = \left[\left(\frac{\partial \mathbf{a}^o}{\partial \mathbf{u}^{oT}} \right)^T \quad \left(\frac{\partial \mathbf{r}^o}{\partial \mathbf{u}^{oT}} \right)^T \right]^T. \tag{84}$$

$\left(\frac{\partial \mathbf{a}^o}{\partial \mathbf{u}^{oT}} \right)^T$ has been evaluated above. The derivative of an element of $\mathbf{r}^o$ with respect to $\mathbf{u}^{oT}$ is

$$\frac{\partial r_{i1}^o}{\partial \mathbf{u}^{oT}} = \frac{(\mathbf{u}^o - \mathbf{s}_i)^T}{r_i^o} - \frac{\mathbf{u}^{oT}}{r^o}. \tag{85}$$

Appendix B

In the hybrid AOA-TDOA model, we have from (55)

$$\bar{\mathbf{J}}'_f(\boldsymbol{\zeta}^o) = \bar{\mathbf{J}}'_{f,a}(\boldsymbol{\zeta}^o) + \bar{\mathbf{J}}'_{f,r}(\boldsymbol{\zeta}^o), \tag{86}$$

$$\bar{\mathbf{J}}''_f(\boldsymbol{\zeta}^o) = \bar{\mathbf{J}}''_{f,a}(\boldsymbol{\zeta}^o) + \bar{\mathbf{J}}''_{f,r}(\boldsymbol{\zeta}^o). \tag{87}$$

Similarly, due to the uncorrelated behavior of the AOA and TDOA noise in the measurement model,

$$E[\Delta \mathbf{J}''^T_f \Delta \mathbf{J}'_f] = E[\Delta \mathbf{J}''^T_{f,a} \Delta \mathbf{J}'_{f,a}] + E[\Delta \mathbf{J}''^T_{f,r} \Delta \mathbf{J}'_{f,r}]. \tag{88}$$

We can expand (6) as

$$J_{f,a} = \sum_{i,j=1}^{M} w_{i,j}(\theta_i - \theta)(\theta_j - \theta) + \sum_{i,j=1}^{M} w_{M+i,M+j} (\phi_i - \phi)(\phi_j - \phi) + 2 \sum_{i,j=1}^{M} w_{i,M+j}(\theta_i - \theta)(\phi_j - \phi), \tag{89}$$

$$\frac{\partial \cos\varphi_j^o}{\partial \boldsymbol{\zeta}^o} = \begin{bmatrix} -\cos\alpha_j \sin\theta^o \cos\beta_j \cos\phi^o + \sin\alpha_j \cos\theta^o \cos\beta_j \cos\phi^o \\ -\cos\alpha_j \cos\theta^o \cos\beta_j \sin\phi^o - \sin\alpha_j \sin\theta^o \cos\beta_j \sin\phi^o + \sin\beta_j \cos\phi^o \end{bmatrix}. \tag{99}$$

where $w_{i,j}$ is the (i, j)-th element of $\mathbf{Q}_{\mathbf{m}}^{-1}$. The mean of the Jacobian matrix of $J_{f,a}$ is

$$\bar{\mathbf{J}}'_{f,a}(\boldsymbol{\zeta}^o) = \begin{bmatrix} -2\sum_{i,j=1}^{M} w_{i,j}(\theta_i^o - \theta^o) - 2\sum_{i,j=1}^{M} w_{i,M+j}(\phi_j^o - \phi^o) \\ -2\sum_{i,j=1}^{M} w_{M+i,M+j}(\phi_i^o - \phi^o) - 2\sum_{i,j=1}^{M} w_{i,M+j}(\theta_i^o - \theta^o) \end{bmatrix} \tag{90}$$

and that of the Hessian is

$$\bar{\mathbf{J}}''_{f,a}(\boldsymbol{\zeta}^o) = \begin{bmatrix} 2\sum_{i,j=1}^{M} w_{i,j} & 2\sum_{i,j=1}^{M} w_{i,M+j} \\ 2\sum_{i,j=1}^{M} w_{i,M+j} & 2\sum_{i,j=1}^{M} w_{M+i,M+j} \end{bmatrix}. \tag{91}$$

Also,

$$\Delta\mathbf{J}'_{f,a}(\boldsymbol{\zeta}^o) = \begin{bmatrix} -2\sum_{i,j=1}^{M} w_{i,j} n_i - 2\sum_{i,j=1}^{M} w_{i,M+j} n_{M+j} \\ -2\sum_{i,j=1}^{M} w_{M+i,M+j} n_{M+i} - 2\sum_{i,j=1}^{M} w_{i,M+j} n_i \end{bmatrix} \tag{92}$$

and

$$\Delta\mathbf{J}''_{f,a}(\boldsymbol{\zeta}^o) = 0 \tag{93}$$

where n_i is the i-th element of the hybrid measurement noise vector $\mathbf{n}$.

For the TDOA component, using (57) gives

$$\bar{\mathbf{J}}'_{f,r}(\boldsymbol{\zeta}^o) = 2\sum_{i,j=2}^{M} w_{2M+i-1,2M+j-1}(r_{i1}^o + R_i\cos\varphi_i^o) R_j \frac{\partial \cos\varphi_j^o}{\partial \boldsymbol{\zeta}^o}, \tag{94}$$

$$\bar{\mathbf{J}}''_{f,r}(\boldsymbol{\zeta}^o) = 2\sum_{i,j=2}^{M} w_{2M+i-1,2M+j-1} R_i R_j \frac{\partial \cos\varphi_i^o}{\partial \boldsymbol{\zeta}^o}\frac{\partial \cos\varphi_j^o}{\partial \boldsymbol{\zeta}^{oT}} + 2\sum_{i,j=2}^{M} w_{2M+i-1,2M+j-1}(r_{i1}^o + R_i\cos\varphi_i^o) R_j \frac{\partial^2 \cos\varphi_j^o}{\partial \boldsymbol{\zeta}^o \partial \boldsymbol{\zeta}^{oT}}, \tag{95}$$

$$\Delta\mathbf{J}'_{f,r}(\boldsymbol{\zeta}^o) = 2\sum_{i,j=2}^{M} \omega_{2M+i-1,2M+j-1} R_i \frac{\partial \cos\varphi_i^o}{\partial \boldsymbol{\zeta}^o} n_{2M+j-1}, \tag{96}$$

and

$$\Delta\mathbf{J}''_{f,r}(\boldsymbol{\zeta}^o) = 2\sum_{i,j=2}^{M} \omega_{2M+i-1,2M+j-1} R_i \frac{\partial^2 \cos\varphi_i^o}{\partial \boldsymbol{\zeta}^o \partial \boldsymbol{\zeta}^{oT}} n_{2M+j-1}. \tag{97}$$

As a result,

$$E[\Delta\mathbf{J}''^T_f \Delta\mathbf{J}'_f] = E[\Delta\mathbf{J}''^T_{f,r} \Delta\mathbf{J}'_{f,r}] = 4\sum_{i,j=2}^{M} \omega_{2M+i-1,2M+j-1} R_i R_j \frac{\partial^2 \cos\varphi_i^o}{\partial \boldsymbol{\zeta}^o \partial \boldsymbol{\zeta}^{oT}} \frac{\partial \cos\varphi_j^o}{\partial \boldsymbol{\zeta}^o}. \tag{98}$$

We can easily obtain $\frac{\partial \cos\varphi_j^o}{\partial \boldsymbol{\zeta}^o}$ and $\frac{\partial^2 \cos\varphi_i^o}{\partial \boldsymbol{\zeta}^o \partial \boldsymbol{\zeta}^{oT}}$ from (58). The first order derivative is (99), as shown at top of this page.

The second order derivative is

$$\frac{\partial^2 \cos\varphi_i^o}{\partial \boldsymbol{\zeta}^o \partial \boldsymbol{\zeta}^{oT}} = \begin{bmatrix} \frac{\partial^2 \cos\varphi_i^o}{\partial \theta^{o2}} & \frac{\partial^2 \cos\varphi_i^o}{\partial \theta^o \partial \phi^o} \\ \frac{\partial^2 \cos\varphi_i^o}{\partial \theta^o \partial \phi^o} & \frac{\partial^2 \cos\varphi_i^o}{\partial \phi^{o2}} \end{bmatrix}, \tag{100}$$

where

$$\frac{\partial^2 \cos\varphi_i^o}{\partial \theta^{o2}} = -cos\alpha_i \cos\theta^o \cos\beta_i \cos\phi^o - \sin\alpha_i \sin\theta^o \cos\beta_i \cos\phi^o, \tag{101}$$

$$\frac{\partial^2 \cos\varphi_i^o}{\partial \theta^o \partial \phi^o} = \cos\alpha_i \sin\theta^o \cos\beta_i \sin\phi^o - \sin\alpha_i \cos\theta^o \cos\beta_i \sin\phi^o, \tag{102}$$

$$\frac{\partial^2 \cos\varphi_i^o}{\partial \phi^{o2}} = -\cos\alpha_i \cos\theta^o \cos\beta_i \cos\phi^o - \sin\alpha_i \sin\theta^o \cos\beta_i \cos\phi^o - \sin\beta_i \sin\phi^o. \tag{103}$$

REFERENCES

[1] C. Liu *et al.*, "RSS distribution-based passive localization and its application in sensor networks," *IEEE Trans. Wireless Commun.*, vol. 14, no. 4, pp. 2883–2895, Apr. 2016.

[2] H. Ramos, A. Boukerche, R. Pazzi, A. Frery, and A. Loureiro, "Cooperative target tracking in vehicular sensor networks," *IEEE Trans. Wireless Commun.*, vol. 19, no. 5, pp. 66–73, Oct. 2012.

[3] A. E. Assaf, S. Zaidi, S. Affes, and N. Kandil, "Low-cost localization for multihop heterogeneous wireless sensor networks," *IEEE Trans. Wireless Commun.*, vol. 15, no. 1, pp. 472–484, Jan. 2016.

[4] H. Hur and H.-S. Ahn, "Discrete-time H_∞ filtering for mobile robot localization using wireless sensor network," *IEEE Sensors J.*, vol. 13, no. 1, pp. 245–252, Jan. 2013.

[5] K. Yan, H.-C. Wu, and S. S. Iyengar, "Robustness analysis and new hybrid algorithm of wideband source localization for acoustic sensor networks," *IEEE Trans. Wireless Commun.*, vol. 9, no. 6, pp. 2033–2043, Jun. 2010.

[6] N. Decarli, F. Guidi, and D. Dardari, "A novel joint RFID and radar sensor network for passive localization: Design and performance bounds," *IEEE J. Sel. Topics Signal Process.*, vol. 8, no. 1, pp. 80–95, Feb. 2014.

[7] N. Deshpande, E. Grant, and T. C. Henderson, "Target localization and autonomous navigation using wireless sensor networks—A pseudogradient algorithm approach," *IEEE Syst. J.*, vol. 8, no. 1, pp. 93–103, Mar. 2014.

[8] D.-C. Chang and M.-W. Fang, "Bearing-only maneuvering mobile tracking with nonlinear filtering algorithms in wireless sensor networks," *IEEE Syst. J.*, vol. 8, no. 1, pp. 160–170, Mar. 2014.
[9] W. Zhang, Q. Yin, H. Chen, F. Gao, and N. Ansari, "Distributed angle estimation for localization in wireless sensor networks," *IEEE Trans. Wireless Commun.*, vol. 12, no. 2, pp. 527–537, Feb. 2013.
[10] R. Peng and M. L. Sichitiu, "Angle of arrival localization for wireless sensor networks," in *Proc. IEEE SECON*, Reston, VA, USA, Sep. 2006, pp. 374–382.
[11] Y. Wang and K. C. Ho, "An asymptotically efficient estimator in closed-form for 3-D AOA localization using a sensor network," *IEEE Trans. Wireless Commun.*, vol. 14, no. 12, pp. 6524–6535, Dec. 2015.
[12] L. Lu and H.-C. Wu, "Novel robust direction-of-arrival-based source localization algorithm for wideband signals," *IEEE Trans. Wireless Commun.*, vol. 11, no. 11, pp. 3850–3859, Nov. 2012.
[13] W. H. Foy, "Position-location solutions by Taylor-series estimation," *IEEE Trans. Aerosp. Electron. Syst.*, vol. AES-12, no. 2, pp. 187–194, Mar. 1976.
[14] M. Li and Y. Lu, "Angle-of-arrival estimation for localization and communication in wireless networks," in *Proc. 16th Eur. Signal Process. Conf. (EUSIPCO)*, Lausanne, Switzerland, Aug. 2008, pp. 1–5.
[15] K. Dogancay, "Emitter localization using clustering-based bearing association," *IEEE Trans. Aerosp. Electron. Syst.*, vol. 41, no. 2, pp. 525–536, Apr. 2005.
[16] V. Cevher and J. H. McClellan, "Acoustic node calibration using a moving source," *IEEE Trans. Aerosp. Electron. Syst.*, vol. 42, no. 2, pp. 585–600, Apr. 2006.
[17] M. Hurtado and A. Nehorai, "Performance analysis of passive low-grazing-angle source localization in maritime environments using vector sensors," *IEEE Trans. Aerosp. Electron. Syst.*, vol. 43, no. 2, pp. 780–789, Apr. 2007.
[18] C. Wang, F. Qi, G. Shi, and X. Wang, "Convex combination based target localization with noisy angle of arrival measurements," *IEEE Wireless Commun. Lett.*, vol. 3, no. 1, pp. 14–17, Feb. 2014.
[19] O. Jean and A. J. Weiss, "Geolocation by direction of arrival using arrays with unknown orientation," *IEEE Trans. Signal Process.*, vol. 62, no. 12, pp. 3135–3142, Jun. 2014.
[20] J. Wang, J. Chen, and D. Cabric, "Cramer–Rao bounds for joint RSS/DoA-based primary-user localization in cognitive radio networks," *IEEE Trans. Wireless Commun.*, vol. 12, no. 3, pp. 1363–1375, Mar. 2013.
[21] B. Yao, W. Wang, W. Han, and Q. Yin, "Distributed angle estimation by multiple frequencies synthetic array in wireless sensor localization system," *IEEE Trans. Wireless Commun.*, vol. 13, no. 2, pp. 876–887, Feb. 2014.
[22] Y. T. Chan and K. C. Ho, "A simple and efficient estimator for hyperbolic location," *IEEE Trans. Signal Process.*, vol. 42, no. 8, pp. 1905–1915, Aug. 1994.
[23] G. Wang and H. Chen, "An importance sampling method for TDOA-based source localization," *IEEE Trans. Wireless Commun.*, vol. 10, no. 5, pp. 1560–1568, May 2011.
[24] W. Meng, L. Xie, and W. Xiao, "Optimality analysis of sensor-source geometries in heterogeneous sensor networks," *IEEE Trans. Wireless Commun.*, vol. 12, no. 4, pp. 1958–1967, Apr. 2013.
[25] A. Amar and A. J. Weiss, "Localization of narrowband radio emitters based on doppler frequency shifts," *IEEE Trans. Signal Process.*, vol. 56, no. 11, pp. 5500–5508, Nov. 2008.
[26] A. J. Weiss, "Direct geolocation of wideband emitters based on delay and Doppler," *IEEE Trans. Signal Process.*, vol. 59, no. 6, pp. 2513–2521, Jun. 2011.
[27] T. Tirer and A. J. Weiss, "High resolution direct position determination of radio frequency sources," *IEEE Signal Process. Lett.*, vol. 23, no. 2, pp. 192–196, Feb. 2016.
[28] T. Tirer and A. J. Weiss, "Performance analysis of a high-resolution direct position determination method," *IEEE Trans. Signal Process.*, vol. 65, no. 3, pp. 544–554, Feb. 2017.
[29] C.-D. Wann, "Mobile sensing systems based on improved GDOP for target localization and tracking," in *Proc. IEEE Sensors*, Taipei, Taiwan, Oct. 2012, pp. 1–4.
[30] J. Yin, Q. Wan, S. Yang, and K. C. Ho, "A simple and accurate TDOA-AOA localization method using two stations," *IEEE Signal Process. Lett.*, vol. 23, no. 1, pp. 144–148, Jan. 2016.
[31] Y. Wang and K. C. Ho, "TDOA positioning irrespective of source range," *IEEE Trans. Signal Process.*, vol. 65, no. 6, pp. 1447–1460, Mar. 2017.
[32] J. Liang and D. Liu, "Passive localization of mixed near-field and far-field sources using two-stage MUSIC algorithm," *IEEE Trans. Signal Process.*, vol. 58, no. 1, pp. 108–120, Jan. 2009.
[33] P. Strobach, "Total least squares phased averaging and 3-D ESPRIT for joint azimuth-elevation-carrier estimation," *IEEE Trans. Signal Process.*, vol. 49, no. 1, pp. 54–62, Jan. 2001.
[34] J. S. Abel, "A bound on mean-square-estimate error," *IEEE Trans. Inf. Theory*, vol. 39, no. 5, pp. 1675–1680, Sep. 1993.
[35] A. Bhattacharyya, "On some analogues of the amount of information and their use in statistical estimation," *Sankhyā, Indian J. Statist.*, vol. 8, no. 4, pp. 1–14, 1946.
[36] J. M. Hammersley, "On estimating restricted parameters," *J. Roy. Statist. Soc. B, Methodol.*, vol. 12, no. 2, pp. 192–240, 1950.
[37] D. G. Chapman and H. Robbins, "Minimum variance estimation without regularity assumptions," *Ann. Math. Statist.*, vol. 22, no. 4, pp. 581–586, 1951.
[38] K. C. Ho and Y. T. Chan, "Geolocation of a known altitude object from TDOA and FDOA measurements," *IEEE Trans. Aerosp. Electron. Syst.*, vol. 33, no. 3, pp. 770–783, Jul. 1997.
[39] S. M. Kay, *Fundamentals of Statistical Signal Processing: Estimation Theory*. Upper Saddle River, NJ, USA: Prentice-Hall, 1993.
[40] J. Wang, J. Chen, and D. Cabric, "Stansfield localization algorithm: Theoretical analysis and distributed implementation," *IEEE Wireless Commun. Lett.*, vol. 2, no. 3, pp. 327–330, Jun. 2013.
[41] J. Werner *et al.*, "Sectorized antenna-based DoA estimation and localization: Advanced algorithms and measurements," *IEEE J. Sel. Areas Commun.*, vol. 33, no. 11, pp. 2272–2286, Nov. 2015.

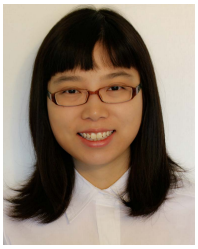

Yue Wang (S'13) received the B.S. degree in electrical engineering and automation from the Beijing Institute of Technology, China, in 2009, and the M.S. degree in electrical and computer engineering from the University of Missouri in 2011, where she is currently pursuing the Ph.D. degree with the Department of Electrical and Computer Engineering. Her current research interests include source localization and sensor array processing.

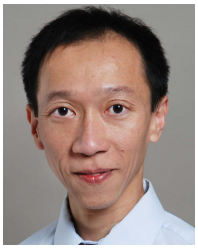

K. C. Ho (S'89–M'91–SM'00–F'09) was born in Hong Kong. He received the B.Sc. degree (Hons.) in electronics in 1988 and the Ph.D. degree in electronic engineering in 1991.

He was a Research Associate with the Royal Military College of Canada, from 1991 to 1994. He joined the Bell-Northern Research, Montreal, Canada, as a Member of Scientific Staff, in 1995. He was a Faculty Member with the Department of Electrical Engineering, University of Saskatchewan, Saskatoon, Canada, from 1996 to 1997. Since 1997, he has been with the University of Missouri, where he is currently a Professor with the Electrical Engineering and Computer Science Department. His research interests are in sensor array processing, source localization, subsurface object detection, wireless communications, and adaptive processing.

Dr. Ho is an inventor of nine patents in the U.S. and 13 patents in Canada, Europe, and Asia on geolocation and signal processing for wireless communications. He was active in the development of the ITU-T Standard Recommendations from 1995 to 2012. He was the Rapporteur of ITU-T Q15/SG16: Voice Gateway Signal Processing Functions and Circuit Multiplication Equipment/Systems from 2009 to 2012, and the Associate Rapporteur of ITU-T Q16/SG16: Speech Enhancement Functions in Signal Processing Network Equipment in 2012. He was a recipient of the Senior Faculty Research Award in 2014 and 2009, and the Junior Faculty Research Award in 2003 and the Teaching Award in 2006 from the College of Engineering, University of Missouri. He served as the Technical Co-Chair of the IEEE International Conference on Acoustics, Speech and Signal Processing 2016 (ICASSP2016). He was the Vice-Chair from 2011 to 2012, the Chair from 2013 to 2014, and the Past Chair in 2015 of the Sensor Array and Multichannel Technical Committee of the IEEE Signal Processing Society. He served on the organizing committees of the IEEE SAM 2008 Workshop and the IEEE CAMSAP 2011. He was an Editor of the ITU-T Recommendations G.168: Digital Network Echo Cancellers from 2000 to 2012, G.799.2: Mechanism for Dynamic Coordination of Signal Processing Network Equipment from 2004 to 2009, and G.160: Voice Enhancement Devices from 2006 to 2012. He was an Associate Editor of the IEEE TRANSACTIONS ON SIGNAL PROCESSING, from 2009 to 2013 and from 2003 to 2006, and the IEEE SIGNAL PROCESSING LETTERS, from 2004 to 2008.